ACS Catalysis

Research Article

pubs.acs.org/acscatalysis

Controlling Nanoscale Properties of Supported Platinum Catalysts through Atomic Layer Deposition

Troy D. Gould, Alia M. Lubers, April R. Corpuz, Alan W. Weimer, John L. Falconer, and J. Will Medlin*

Department of Chemical and Biological Engineering, University of Colorado, Boulder, Colorado 80309, United States

Supporting Information

ABSTRACT: Platinum nanoparticles were grown on alumina by atomic layer deposition using either H_2 or O_2 as the second half-reaction precursor. Particle diameters could be tuned between ~1 and 2 nm by varying between use of H_2 and O_2 and by changing the number of ALD cycles. The use of H_2 as the second precursor led to smaller Pt particle sizes. Differences in particle size were found to be related to the availability of surface hydroxyl groups, which were monitored via in situ infrared spectroscopy during Pt ALD. Temperature-programmed desorption (TPD) of CO and diffuse reflectance infrared Fourier transform spectroscopy (DRIFTS) for adsorbed CO were used to characterize sites and coordination numbers of the nanoparticles. As expected, smaller nanoparticles had sites with lower average coordination numbers. The catalysts were evaluated for oxidative dehydrogenation of propane to propylene. Catalysts having the smallest Pt particles with the lowest coordination number (synthesized by one cycle of Pt ALD with H_2) had a C_3H_6 selectivity of 37% at 14% conversion, whereas under the same reaction conditions the selectivity was less than 1% for larger (3.6 nm) commercial Pt catalysts at 9% conversion.

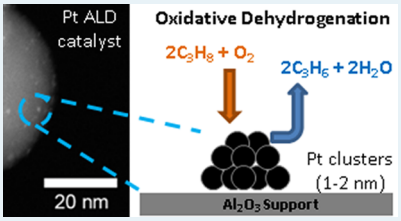

KEYWORDS: *atomic layer deposition, oxidative dehydrogenation, platinum, nanoparticles, heterogeneous catalysis*

INTRODUCTION

A major focus in catalysis research is advancing toward precise control of nanometer and subnanometer features in catalytic materials. These advances have been made possible by new synthesis methods, better analytical techniques to probe ultrasmall features, and a greater understanding of fundamental catalytic principles at the nanoscale through theoretical investigations.[1−3] One example of a highly sought after reaction is oxidative dehydrogenation (ODH) of alkanes to alkenes, which can benefit from advances in nanostructured catalysts.[4] Oxidative dehydrogenation of propane (ODHP) to propylene is of particular interest. The global demand for propylene is expected to increase by more than 20 billion kilograms by 2017, with global sales currently exceeding $90 billion US.[5] Propylene is primarily produced in steam crackers, with a smaller fraction produced in fluid catalytic cracking (FCC) units, and an even smaller fraction produced by catalytic dehydration.[6] The cracking processes are highly endothermic, require regeneration of the catalysts due to coking, and produce fractions of ethylene larger than those of propylene.[7] Oxidative dehydrogenation, in contrast, can be operated at temperatures below 773 K and is exothermic.[7] Currently, ODHP catalysts do not have high enough yields to cause propylene manufacturers to adopt ODHP as a viable alternative over traditional cracking technologies.

Oxidative dehydrogenation is known as a type III structure-sensitive reaction: i.e., the turnover frequency increases as the particle size decreases.[8,9] Vajda et al. used density functional theory (DFT) to elucidate why this reaction became more favorable on Pt clusters of 4−8 atoms.[9] Clusters of this size have atoms with a coordination number (CN) of 3 to 4, and their study showed that these atoms have a barrier for breaking a C−H bond lower than that for breaking a C−C bond to form CO or CO_2. Supported Pt catalysts with larger crystallite sizes and Pt(111) surfaces have shown minimal selectivity to propylene and instead catalyze combustion, favoring C−C bond breaking over C−H bond breaking.[10] However, size-selected Pt clusters of 8−10 atoms have achieved propylene selectivities greater than 60%. Those catalysts were prepared with a technique requiring a continuous cluster beam as the Pt source.[9]

Atomic layer deposition (ALD) has been used in the past decade because of its ability in some applications to prepare small Pt nanoclusters. Although liquid-phase catalyst preparation can achieve more precise control over size and shape,[11,12] the solvents are often hazardous, and the synthesis requires further steps to purify the product, cleave organic capping agents, and deposit the separately prepared particles on a support.[11,13,14] Aaltonen et al. pioneered the use of trimethyl(methylcyclopentadienyl)platinum (Me_3(MeCp)Pt) and O_2 to deposit Pt films using hundreds of Pt ALD cycles.[15] Since that time, this oxidative ALD process has been used to deposit Pt nanoparticles using a range of numbers of cycles and various metal oxide supports.[16−19] In situ FTIR of gas-phase ALD products and X-ray absorption techniques have been used to gain a better understanding of the ALD mechanism.[19,20] The generally accepted mechanism for Pt ALD, once a sufficient amount of Pt is deposited, is as follows for the O_2 chemistry.[20]

Received: August 25, 2014
Revised: December 7, 2014
Published: January 12, 2015

DOI: 10.1021/cs501265b
ACS Catal. 2015, 5, 1344−1352

The first half-reaction, dosing the Pt precursor, is

$$2(\mathrm{MeCp})\mathrm{PtMe_3}(g) + 3\mathrm{O}(\mathrm{ads}) \rightarrow 2(\mathrm{MeCp})\mathrm{PtMe_2}(\mathrm{ads}) + \mathrm{CH_4}(g) + \mathrm{CO_2}(g) + \mathrm{H_2O}(g)$$

The second half-reaction, using O_2, is

$$2(\mathrm{MeCp})\mathrm{PtMe_2}(\mathrm{ads}) + 24\mathrm{O_2}(g) \rightarrow 2\mathrm{Pt}(s) + 3\mathrm{O}(\mathrm{ads}) + 16\mathrm{CO_2}(g) + 13\mathrm{H_2O}(g)$$

This reaction mechanism is operable once Pt particles or layers are already deposited. However, in the first few cycles, the active sites for deposition on metal oxides are OH groups. As the number of ALD cycles increases, the Pt coverage increases until the active sites for deposition are exclusively Pt−O.[19] Alternatively, instead of O_2 as the precursor in the second half-reaction, H_2 can be used to hydrogenate the organic groups of the Pt precursor. No Pt−O species form when H_2-based ALD is used, and the active sites are the OH groups on the surface of the metal oxide.[19]

The focus on creating ultrasmall, isolated Pt nanoparticles or nanoclusters has encouraged several theoretical studies that investigated the mechanisms of single Pt and Pd adatom behavior on metal oxide support surfaces. Diffusion via site-to-site transitions has been studied on γ-alumina for both Pt and Pd atoms through DFT.[21,22] Interestingly, hydroxyl groups adsorbed on Al_2O_3 decrease the adsorption strength of Pt and Pd atoms on the support but drastically increase the diffusion barriers of metal atoms on these surfaces. For Pd atom diffusion, Valero et al. showed that a hydroxylated surface caused the low-energy diffusion trajectory barrier to increase by as much as 74 kJ/mol.[22] These OH groups may play a significant role in the Pt ALD mechanism, since they are proposed as the active site during H_2 ALD but not during most steps of O_2 ALD.[19]

In the present study, the effect of the second half-reaction chemistry on particle size was investigated with one or five ALD cycles. Changing the number of cycles and reaction chemistry varied the particle size between 1 and 2.5 nm. The difference between H_2 and O_2 ALD during the deposition of Pt on alumina was investigated by in situ Fourier transform infrared (FTIR) spectroscopic characterization of the surface hydroxyl groups. Particle sizes were measured by transmission electron microscopy (TEM) and specific chemisorption, and the surface structures of these catalysts were characterized by CO temperature-programmed desorption (TPD) and CO diffuse reflectance infrared Fourier transform spectroscopy (DRIFTS), with an emphasis on characterizing low-coordinated atoms. Finally, these catalysts were evaluated for activity and selectivity for ODHP.

EXPERIMENTAL METHODS

ALD Synthesis. Platinum particles were synthesized on alumina supports by ALD using either a stainless steel fluidized bed reactor (FBR) for 2 g batches, as described elsewhere,[23,24] or a quartz tube FBR (6 mm inner diameter) with a quartz glass frit of 40 μm pore size that supported the powder bed for smaller batches. The alumina powder was fluidized in the quartz reactor at approximately 0.25 Pa pressure with He carrier gas flow rates of 5−20 sccm (standard cubic centimeter per minute). The alumina was then dried for 2 h under vacuum at 393 K before Pt was deposited by ALD in the quartz FBR. Both porous alumina (Albermarle MARTOXID AN/I γ-alumina) and nonporous nanosphere alumina (Aldrich 544833 γ-alumina) were used as supports. Platinum was deposited at 448 K, which is much lower than the 573 K temperature typically used for Pt ALD with $Me_3(MeCp)Pt$ and O_2.[17,19,25] In this work, either H_2 (Airgas 20% H2, balance Ar) or O_2 (research grade, Airgas) was used as the second reagent for Pt ALD.

Catalyst Characterization. The catalysts were characterized by TPD in a quartz tube reactor (6.35 mm inner diameter) at ramp rates of 20 K/min, and the reactor effluent was analyzed with an SRS RGA 200 mass spectrometer. For CO TPD, the catalysts were reduced for 2 h at 523 K, purged with Ar, flashed to 923 K to desorb residual H_2 and H_2O, cooled to room temperature, dosed with CO (100 sccm 20% CO in Ar) for 10 min, and then purged with Ar before ramping the temperature.

Particle size estimates were obtained using ImageJ software to analyze images from FEI Tecnai 12-Spirit Biotwin TEM, Phillips CM-100 TEM, and JEOL ARM200F TEM instruments. For even higher resolution imaging, bright field images were taken by high-resolution TEM and dark field images were taken by high-angle, annular dark field scanning transmission electron microscopy (HAADF STEM) at the NIST Precision Imaging Facility (PIF) on a JEOL ARM200F microscope with a Shottky field emission gun. Samples were electrostatically adhered to copper grids with a lacey carbon overlayer (Ted-Pella 01895 Lacey Carbon Film grids) to avoid effects of solvents from drop-casting. Samples prepared for imaging purposes were synthesized on the nonporous nanosphere alumina so that the metal catalyst particles were on the surface of the spheres and were visible by TEM. More details about the magnifications used and particle measurements can be found in the Supporting Information. The weight loadings of each sample were determined by inductively coupled plasma mass spectroscopy (ICP-MS). The number of active sites was measured with a Quantachrome AS-1 Autosorb. The catalysts were reduced at 523 K in pure H_2 for 2 h before measuring the H_2 uptake.

A Nicolet 6700 FTIR spectrometer was used to measure spectra at 4 cm^{-1} resolution by transmission IR for in situ ALD experiments, and diffuse reflectance infrared Fourier transform spectroscopy (DRIFTS) was used for CO adsorption experiments. For the in situ ALD measurements, alumina nanopowder was mixed in a 1:2 ratio with KBr and pressed into a tungsten grid with a hydraulic press at approximately 20000 N. The sample was loaded into a vacuum chamber with IR-transparent CaF_2 windows; this chamber is described in more detail elsewhere.[26] A thermocouple was placed within 2 mm of the tungsten grid to monitor the temperature of the grid. Background spectra were collected on the empty IR cell under vacuum. The chamber was evacuated, heated to approximately 400 K, and scanned before the first Pt ALD dose. The Pt, O_2, and H_2 static doses were done for 30 min each; longer dose durations showed no discernible differences. Between each dose the chamber was evacuated for at least 30 min to remove residual precursor molecules. A blank grid loaded with KBr was coated by three cycles of Pt ALD, and the KBr turned black, just as in the experiments with alumina, but with the KBr-only sample, no distinctive IR features were observed at any point during the deposition. The contribution of KBr to the observed FTIR spectra was negligible because the surface area of the KBr

DOI: 10.1021/cs501265b
ACS Catal. 2015, 5, 1344−1352

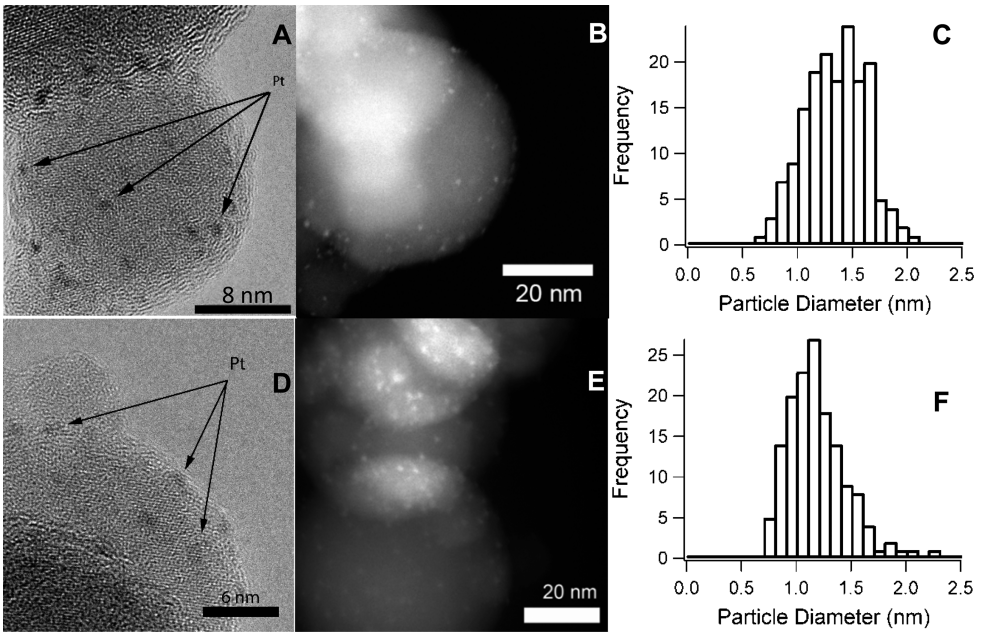

Figure 1. HRTEM, HAADF STEM, and size distribution of Pt nanoparticles synthesized by (A–C) one Pt ALD cycle with O_2 on spherical alumina support and (D–F) one Pt ALD cycle with H_2.

was 0.23 m^2/g, in comparison to 35 m^2/g for the alumina support.

The CO DRIFTS experiments were performed on a bed of catalyst powder using a closed cell attachment (Harrick). Each sample was oxidized for 2 h at 573 K and then reduced at 473 K for 2 h to ensure metallic Pt. Note that the oxidation and reduction temperatures were 30–50 K lower than those used in the reactor studies due to limitations of the apparatus. The catalysts were then loaded into the chamber and degassed under vacuum for several hours to desorb water from the alumina supports. Carbon monoxide was dosed at room temperature at sequentially higher CO pressures until no further changes in IR spectra were detected. For the temperature-ramp DRIFTS study, the sample was initially saturated with CO (at a CO pressure of ~185 kPa), and then the chamber was evacuated and held under vacuum for all CO DRIFTS measurements. The sample was heated from room temperature to 600 K under vacuum in approximately 50 K increments, allowing at least 1 h equilibration time before the spectra were measured for a given temperature.

Catalyst Evaluation. The Pt catalysts were evaluated for their activity and selectivity for ODHP. Prior to exposure to reaction conditions, the catalysts were oxidized at 600 K for 10 min in a 20% O_2 stream at 100 sccm. Then they were reduced in 100 sccm of 20% H_2 for 1 h at 523 K. For most catalytic testing, approximately 100 mg of catalyst was used, resulting in a nearly constant space velocity of 28 s^{-1} and full consumption of the O_2. Reactants flowed through the same packed-bed, quartz tube reactor described above for the TPD studies, and the reactor effluent was measured by a SRI GC 8610c instrument with a Haysep-D packed column. Flow rates for ODHP selectivity studies were 12 sccm of C_3H_8, 6 sccm of O_2, and 182 sccm of Ar. A 5 wt % commercial Pt/Al_2O_3 catalyst (Sigma) was tested for ODHP activity as a basis of comparison to larger, more Pt(111)-terminated Pt particles. Turnover frequencies (TOF) were also measured by running the reaction at less than full O_2 conversion (~50–75% conversion) by using less catalyst (typically 2 mg or less) and diluting the catalyst bed with the same alumina to 100 mg total bed weight. The same inlet concentration of reactants (C_3H_8) was used to determine TOFs, with the number of active sites calculated from H_2 chemisorption dispersion measurements and total metal loading.

RESULTS AND DISCUSSION

Effect of Second Precursor and Number of Cycles on Particle Size. For one Pt ALD cycle at 448 K on the alumina supports, the Pt particles were smaller when H_2 rather than O_2 was used as the second reagent. Images and size distributions are shown in Figure 1. Even though the first Pt ALD half-cycle on alumina was exactly the same, using H_2 in the second half-cycle produced an average Pt cluster size (measured by TEM) of 1.1 ± 0.2 nm, whereas using O_2 produced 1.4 ± 0.2 nm clusters. The difference in average particle size was statistically significant according to a two-sample t test at $\alpha = 0.05$. These particle sizes are similar to those measured by extended X-ray absorption fine structure (EXAFS) by Setthapun et al. for one-cycle Pt ALD on spherical alumina with O_2 and H_2, although they used deposition temperatures of 573 K for the O_2 reaction and 473 K for the H_2 reaction.[19] Each catalyst had essentially the same weight loading of approximately 1.0 wt % (± 0.2%) because the first ALD half-cycle, which deposits the platinum precursor, was the same for the two preparations. The number of active sites per gram of metal measured by chemisorption was larger for the H_2-synthesized particles than for O_2-synthesized particles. The average particle sizes calculated from chemisorption, given in Table 1, were smaller than those obtained from TEM, which may not be able to detect sub-nanometer particles. Additionally, a significant fraction of Pt particles can adsorb more than one H per active site when the average surface CN of the cluster drops below ~6.[27]

We also prepared catalysts with higher Pt weight loading using five ALD cycles. As shown in Figure 2, using H_2 as the second precursor again resulted in smaller particle sizes (1.7 ± 0.4 nm) in comparison to those using O_2 (2.4 ± 0.5 nm). Platinum loadings measured by ICP were identical for the two

DOI: 10.1021/cs501265b
ACS Catal. 2015, 5, 1344–1352

Table 1. Pt Catalyst Properties

catalyst[a]	H_2 adsorbed (μmol $g_{catalyst}^{-1}$)	Pt weight loading (%)	particle size by TEM (nm)	particle size by chemisorption (nm)[b]
1-cycle Pt ALD with O_2	26	1.2	1.4 ± 0.2	1.3
1-cycle Pt ALD with H_2	33	0.94	1.1 ± 0.2	0.8
5-cycle Pt ALD with O_2	74	4.7	2.4 ± 0.5	1.8
5-cycle Pt ALD with H_2	91	4.7	1.7 ± 0.4	1.4
commercial 5 wt % Al_2O_3	40	5	3.9 ± 1.1	3.6

[a]The ALD catalysts were synthesized on nonporous nanopshere alumina. [b]Values for chemisorption were calculated assuming a H:Pt ratio of 1, but this assumption breaks down at high dispersions because a significant fraction of surface Pt atoms can adsorb more than 1 H atom per Pt site in this size range.[27] These values therefore represent a minor underestimation of particle size.

samples at approximately 4.7 wt %. Analysis by TEM revealed that some alumina support particles had no Pt nanoparticles, indicating that the Pt particles were not uniformly distributed. Average particle size, weight loadings, and chemisorption values are given in Table 1.

In Situ FTIR during ALD. The relative OH concentration during Pt ALD was measured via in situ FTIR for both H_2 and O_2 ALD chemistry. Figure 3a shows spectra collected following each half cycle when H_2 was used as the second-cycle reactant. The OH stretching band (the broad peak at ~3500 cm^{-1}) did not change much after the first half-cycle. To ensure the surface was saturated, the precursor was statically dosed into the chamber for 30 min, and further exposure (up to 3 h) did not change the IR signal. Scans after subsequent cycles indicated more significant losses of hydroxyl groups, as shown in Figure 3A. During the third Pt ALD cycle (not shown), the overall signal dropped to less than 0.1% transmittance because the Pt increased the opacity of the sample. The sample grid was metallic and black after Pt ALD, whereas the original alumina/KBr powder was completely white. Carbonaceous species (2800−2900 cm^{-1} C−H stretching regions) were also present on the sample during most cycles, but these features were more prominent after the Pt doses (as expected from the organic groups of the precursor). Spectral noise at wavenumbers greater than 3500 cm^{-1} was due to gas-phase water outside the in situ vessel. Our direct monitoring of surface OH groups supports the mechanism proposed by Setthapun et al.[19] that Pt deposits on OH groups after the first cycle when H_2 is used.[19] Interestingly, during the H_2 doses, the OH groups also decreased in concentration. Because alumina is inactive for hydrogen dissociation at these temperatures, these losses were likely from H_2 dissociating on the Pt and then recombining with surface OH groups to form water.

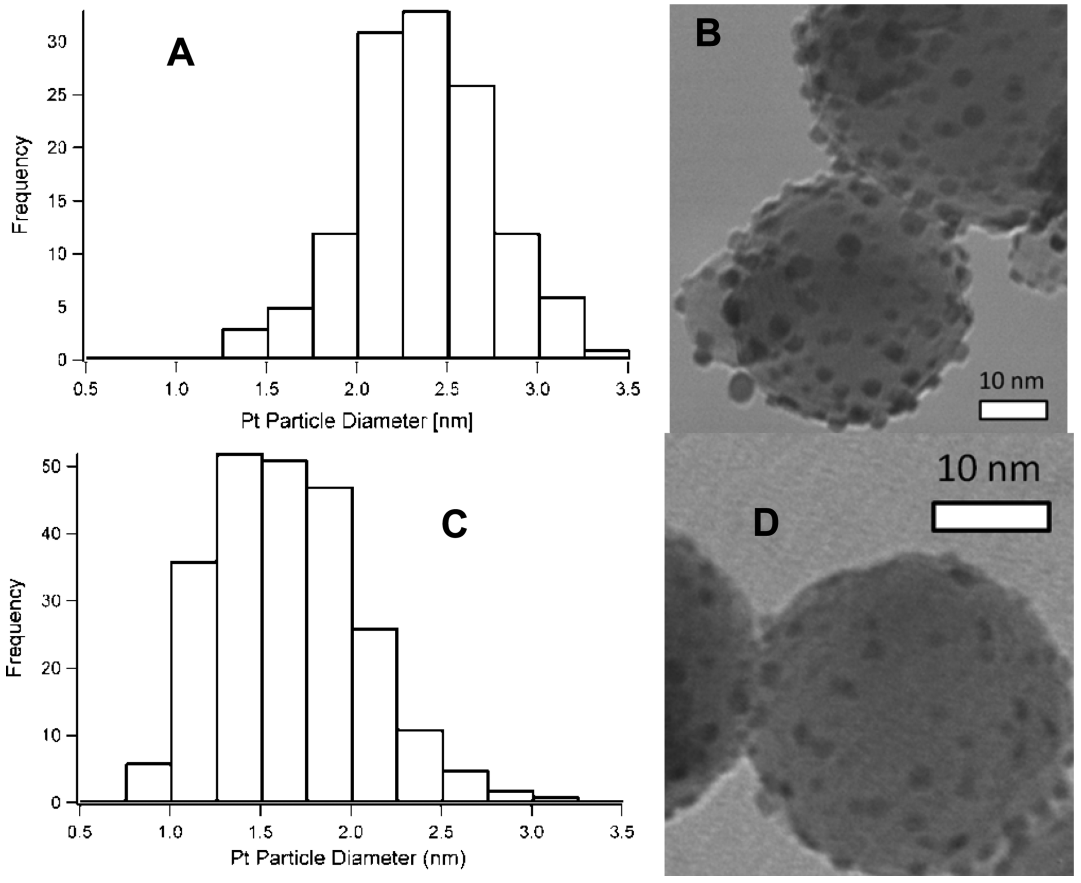

Figure 2. Particle size distribution and TEM image of Pt nanoparticles synthesized on a spherical nanoalumina support by (A, B) five cycles of Pt ALD with O_2 and (C, D) Pt particles synthesized by five cycles of Pt ALD with H_2.

DOI: 10.1021/cs501265b
ACS Catal. 2015, 5, 1344−1352

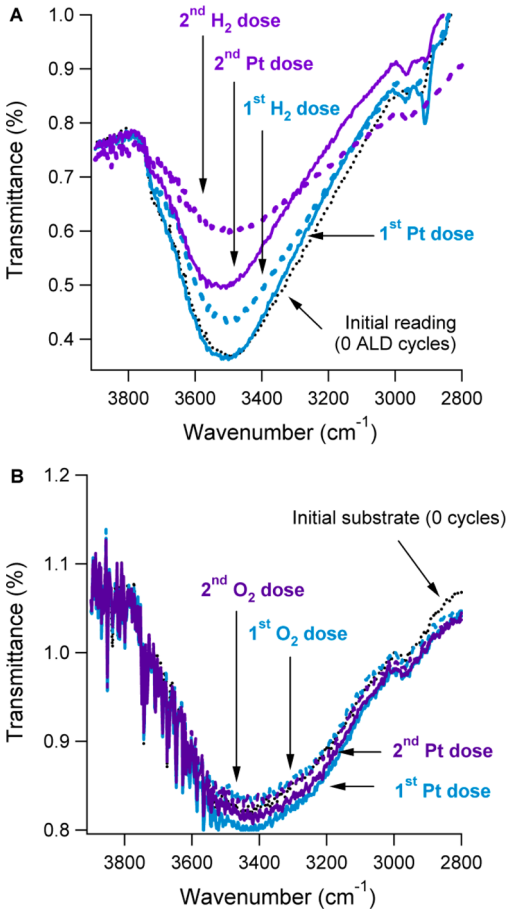

Figure 3. In situ Pt ALD FTIR spectra with (A) H_2 used as the second precursor and (B) O_2 used as the second precursor.

When O_2 was used as the second ALD reagent, no discernible differences in hydroxyl groups were detected with additional ALD cycles (Figure 3B). As with the H_2 chemistry, the sample became opaque due to Pt deposition after three cycles. Platinum was confirmed to be deposited on the sample by visual examination and ICP. The nearly constant OH group concentration indicates the Pt ALD with O_2 serves to (re)oxidize the surface to form a nearly constant level of surface hydroxyls, in contrast to the case of ALD with H_2, where hydroxyl groups are not replenished. Overall this supports the O_2-based Pt ALD mechanism proposed by Setthapun et al.,[19] who suggested that, halfway through the second cycle, new $PtMe_3(MeCp)$ molecules start bonding to Pt−O species instead of (or in addition to) OH groups on the alumina support. They observed this trend from the Pt EXAFS spectrum, with no direct measurement of the OH groups, but here we monitored the OH concentration and arrive at a similar conclusion.

Scheme 1 shows a simple mechanism that is consistent with our results and with those of prior studies.[19] We propose that the smaller particle sizes observed during ALD with H_2 are due to two effects: (i) H_2 produces reduced Pt nanoclusters, which are not effective nucleation sites in subsequent ALD cycles, and (ii) H_2 avoids the replenishment of surface hydroxyl groups during removal of the organic ligand from the Pt precursor. The replenishment of hydroxyl groups may affect both the density of new nucleation sites and the diffusion rates of Pt species on the alumina surface.[21,22] The precise manner in which surface

Scheme 1. Reaction Scheme for Metal Island Growth during Pt ALD with O_2 or H_2, with Active Sites Shown in Blue[a]

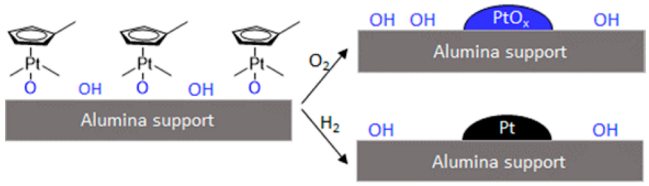

[a]Use of O_2 replenishes surface OH groups on the support and produces oxidized nanoparticles that may serve as nucleation centers. Hydrogen, on the other hand, does not replenish hydroxyls and forms reduced nanoparticles that cannot serve as nucleation centers for subsequent cycles.

hydroxyl groups influence Pt deposition is not clear; note that in the initial Pt dose (Figure 3A) the hydroxyl group density remained essentially constant, suggesting that Pt deposition cannot be tied directly to hydroxyl consumption. More generally, our results suggest that nucleation of new Pt centers during ALD is strongly affected by the presence of oxygenated centers during the precursor exposure; this dependence is commonly observed for a wide variety of ALD chemistries.[28]

Probing Surface Structure by CO DRIFTS and CO TPD. The surface structure of the Pt nanoparticles was probed with CO using DRIFT spectroscopy and TPD. Catalysts were prepared on porous supports for use in the reactor studies and the CO DRIFTS experiments, and their weight loadings and chemisorption H_2 uptake values are given in Table 2.

Table 2. Catalyst Properties for Pt ALD Deposited on Porous Al_2O_3

catalyst	H_2 adsorbed (μmol $g_{catalyst}^{-1}$)	Pt weight loading (%)	H:Pt ratio (mol of H (mol of Pt_{total})$^{-1}$)
1-cycle Pt ALD with O_2	58	1.4	1.6
1-cycle Pt ALD with H_2	62	1.4	1.7
5-cycle Pt ALD with O_2	167	7.4	0.9
5-cycle Pt ALD with H_2	103	3.9	1.3

The Pt particles deposited on the porous supports were in general smaller (based on chemisorption measurements) than those prepared on the nanosphere alumina. The largest particles were synthesized by five cycles of Pt ALD with O_2, with Pt particle diameters calculated to be ~1.3 nm, using the chemisorption values and assuming a H:Pt ratio of 1. However, calculating particle size when the particles approach 100% dispersion results in an underestimation of particle size, since single sites can adsorb more than one H atom and artificially inflate the dispersion calculations.[27] Therefore, particle sizes calculated from chemisorption are not reported for the Pt particles on the porous support. As the particle size decreases, the ability for undercoordinated Pt to adsorb more than one H atom per active site increases, and therefore the H:Pt ratio increases with decreasing particle size.[27] The H:Pt ratio observed for the one-cycle Pt ALD catalyst (with H_2) is in agreement with theoretical H:Pt ratios associated with raft-type Pt clusters of ~10 atoms.[27] The particles may be smaller on the porous support than on the nonporous nanospheres because of differences in OH surface concentration, curvature effects from

DOI: 10.1021/cs501265b
ACS Catal. 2015, 5, 1344−1352

the nanospheres, or diffusion limitations of the Pt precursor on the porous support. Despite the quantitative differences, the general particle size trends were the same on each substrate.

Measuring the size of these small clusters can be challenging, but CO DRIFTS helps elucidate the average coordination number of the Pt clusters. Like the H:Pt ratio, the CO stretching frequency is related to particle size.[29] The two main features in the CO DRIFT spectra were around 1815−1850 and 2040−2075 cm^{-1} (spectra are shown in Figure S1 in the Supporting Information). The peaks around ∼1825 cm^{-1} correspond to bridge-bonded CO, whereas the other feature corresponds to CO linearly bonded to an atop site at a step edge,[30] and linearly bonded CO on a terrace site typically occurs for Pt(111) around 2065−2100 cm^{-1}. The CO stretching frequencies for the catalysts are plotted against H:Pt ratio in Figure 4. This figure shows that the CO stretching

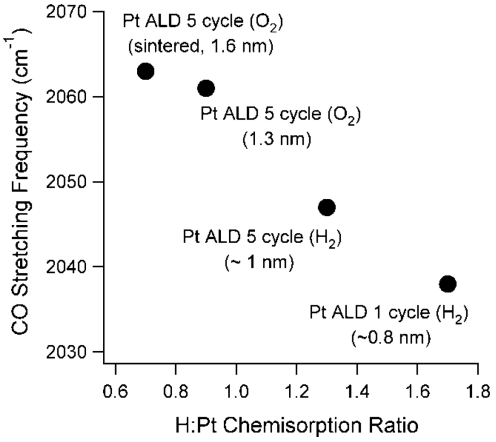

Figure 4. Carbon monoxide stretching frequencies from DRIFTS as a function of H:Pt ratios from chemisorption for several ALD catalysts. Particle sizes were calculated by chemisorption for the O_2-prepared samples and by correlation of the CO DRIFT frequencies to coordination number (and ultimately particle size) for the H_2-prepared samples.

frequency decreases as the H:Pt ratio increases, with both trends corresponding to a decreased particle size. The frequencies reported in Figure 4 were measured at a CO pressure of ∼180 Pa or higher, where the surface was saturated with CO. Results at lower CO pressure are reported in the Supporting Information. The prominent step-site IR feature of the ALD catalysts indicates that the concentration of step sites and other undercoordinated sites was high on these ∼1.0 nm particles. Additionally, the bridge-bonded CO feature (around 1850 cm^{-1}) was minimal for the ALD catalysts because the particles were too small to have many sites on which CO could form a bridge conformation. Kappers and van der Maas investigated the variation of CO frequencies with coordination of Pt atoms, and assigned a coordination number of 5 to a CO adsorption peak at 2035 cm^{-1},[29] which is nearly identical to the peak location for the Pt catalyst produced from one ALD cycle with H_2. Additionally, the peak at 2047 cm^{-1} corresponds to an average coordination number of 6 for the five-cycle ALD sample. De Graaf et al. modeled Pt coordination number as a function of number of atoms in a cluster and particle size.[31] The coordination numbers obtained from FTIR combined with De Graaf's modeling corresponds to a particle size of ∼0.8 nm for the one-cycle Pt ALD (with H_2) catalyst and ∼1 nm for the five-cycle Pt ALD (with H_2) catalyst. A sample of the five-cycle Pt ALD (O_2) catalyst was intentionally sintered to 1.6 nm (by treating in 100% H_2 for 4 h at 873 K) to show the effect of slightly larger particles in the CO DRIFTS experiments and for catalytic evaluation.

The structures of the catalysts were further probed by CO-TPD. The study by Lundwall et al. investigated particle sizes from 2.5 to >4 nm using a similar technique.[32] In the current study, particles with a smaller size (∼1 nm) were investigated, and the CO TPD profiles are shown in Figure 5A. The

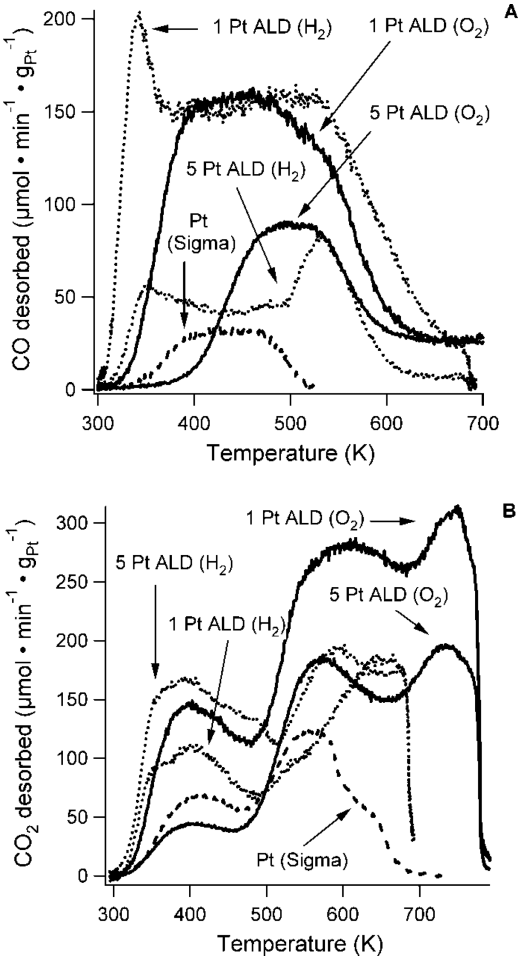

Figure 5. Carbon monoxide TPD of Pt catalysts with different particle sizes: (A) CO desorption; (B) CO_2 desorption.

commercial 5 wt % Pt catalyst had a broad peak that is most likely composed of two separate peaks, one near 400 K corresponding to terrace site desorption and one near 475 K corresponding to step-site desorption. These two desorption modes were also identified by Lundwall et al. for similarly sized Pt particles.[32] All of the ALD catalysts showed significant CO desorption above the 525 K temperature at which desorption on the commercial catalyst was complete. Such higher-temperature desorption modes are often attributed to associative desorption on corner, edge, and kink sites.[33] Surprisingly, the ALD catalysts made with H_2 each had a low-temperature peak around 350 K that was not present for the other catalysts. Only terrace and step site desorption was observed by Lundwall et al., but their particle diameters were at least 2.5 nm and therefore had a lower concentration of edges and corners than the ALD catalysts used in this study. Lower-coordinated atoms increase π back-bonding, which strengthens

DOI: 10.1021/cs501265b
ACS Catal. 2015, 5, 1344−1352

the binding energy of CO on Pt, and red-shifts the CO stretching frequency, as seen in Figure 4. We note that previous studies have found that ALD-prepared catalyst particles can undergo sintering during annealing for several hours in air to 720 K, so that at the highest temperatures in the TPD experiments some sintering cannot be excluded.[17]

Higher desorption temperatures (~500 K) have been observed during CO TPD in UHV on stepped Pt,[34,35] and desorption at ~400 K is also observed during CO TPD of Pt particles supported on γ-alumina.[33,36] Previous studies have noted that very small Pt nanoparticles (or single atoms) exhibit strong perturbations to adsorption and catalytic properties due to both their small size and strong interactions with Al^{3+} cations on the support.[37,38] Thus, the unique CO adsorption properties may also be related to support effects. The desorption peak at ~350 K has rarely been observed but could be similar to the β_1 desorption from Pt(110) observed by McCabe and Schmidt.[39] Overall, the complex desorption behavior observed for the ALD samples is likely to be due to a combination of effects that is difficult to deconvolve. However, the consistent finding of strongly adsorbed CO states for ALD-prepared catalysts suggests that ALD facilitates the preparation of more highly reactive surface sites.

A significant portion of the adsorbed CO desorbed as CO_2, as shown in Figure 5B. Carbon dioxide can come from two reactions: (1) the water−gas shift reaction where OH groups from the alumina support combine with CO to produce CO_2 and H_2 gas and (2) the Boudard reaction in which CO disproportionates to form CO_2 and surface carbon.[33,36,40] For all catalysts investigated, the higher-temperature CO_2 desorption coincided with H_2 desorption (shown in Figure S3 in the Supporting Information), indicating that the CO_2 desorption proceeded through the water-gas shift reaction pathway at temperatures above ~500 K. The two catalysts synthesized by O_2 ALD exhibited similar desorption modes and formed more CO_2 than the other catalysts. The O_2-synthesized catalysts most likely had a higher concentration of OH groups near the Pt particles to form more CO_2 during the TPD, and the in situ FTIR of O_2-ALD indicated that the OH group concentration did not significantly decrease with ALD cycles. For the catalysts prepared using H_2 as the second precursor, the five-cycle catalyst produced more CO_2 but much less CO than the one-cycle catalyst, with a total desorption yield per Pt atom that was approximately 20% lower per surface Pt atom. The reason for this difference in distribution of products is not immediately apparent.

A temperature-programmed study was also performed in the DRIFTS apparatus for the five-cycle H_2 catalyst, as shown in Figure S4 of the Supporting Information. The broad features associated with the CO vibrational frequencies again suggested the presence of a distribution of different types of sites, and it must be noted that dipole coupling between neighboring adsorbates can complicate spectral analysis. Nevertheless, it was found that increasing the temperature to 500 K resulted in a red shift for the ALD catalyst much larger than that for the commercial catalyst. The peak frequency on the ALD catalyst was decreased to well below 2000 cm^{-1}, which has been assigned to CO adsorbed on atoms with coordination numbers of 3−4.[29]

Catalyst Evaluation for ODHP. The catalysts were screened for C_3H_6 selectivity, shown in Figure 6, by running the ODHP reaction with O_2 as the limiting reagent to reduce combustion of C_3H_8 and C_3H_6. Overall, all the ALD-produced

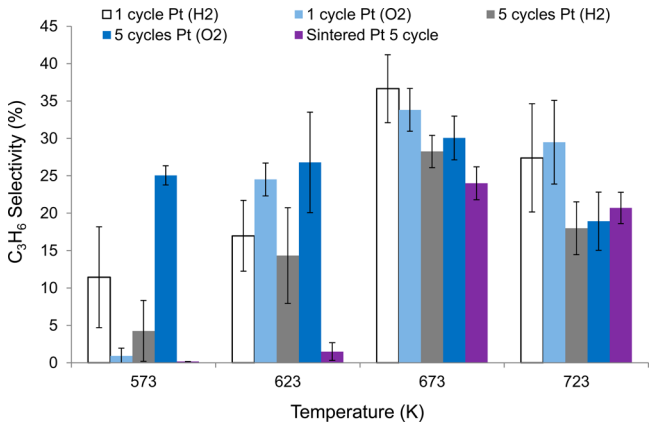

Figure 6. Selectivity to C_3H_6 vs temperature for Pt ALD catalysts in the ODHP reaction. Error bars represent standard deviations from multiple experiments. The same catalyst weight and approximate space velocity were used for all measurements.

catalysts exhibited much higher selectivities than the commercial Pt/Al_2O_3 catalyst due to their smaller Pt particle size. Selectivity to C_3H_6 was below the 1% detection limit for the commercial Pt catalyst with an average particle size of 3.6 nm, whereas selectivities greater than 30% were measured for the smallest particle sizes produced by ALD. The variation in selectivity with temperature agrees with the ODHP experiments by Lei et al., where the selectivity had a maximum of around 673 K.[40] The catalysts with the smallest average particle size (one-cycle Pt ALD with either H_2 or O_2) had the highest selectivities to C_3H_6 at 673 and 723 K, whereas at lower temperatures there were no trends with particle size. While the optimal temperature showed the expected trends with particle size, there were deviations at lower temperatures that may indicate more complexity than directly correlating CN to higher selectivity. The two catalysts prepared with one ALD cycle had almost identical catalytic performances at the highest temperatures since they had similar particle sizes. The best catalyst had a ~5% yield (conversion × selectivity), as shown in Figure S5 in the Supporting Information, similar to a recently reported PtPd bimetallic catalyst for ODHP.[40] The catalysts all stabilized within a 2 h reaction time following a temperature increase and showed no indication of further deactivation once at steady state. An example of the C_3H_6 mass signal versus time is shown in Figure S6 in the Supporting Information. The initial stabilization period may have been due to a combination of particle sintering and coking. To evaluate the importance of sintering, we used TEM to measure the particle size for the sample prepared with five ALD cycles of Pt with H_2 as the second precursor after exposure to reaction conditions for 2 h. The measured particle size (Figure S7 in the Supporting Information) was found to be 1.8 ± 0.5 nm. In comparison to Table 1, this indicates that particle size growth was not significant over the time period associated with activity stabilization.

All of the catalysts that had detectable ODHP activity also produced H_2. Hydrogen production during ODH has been reported recently for a variety of catalysts[7] and can be produced from catalytic dehydrogenation further down the catalyst bed once the O_2 has been exhausted, or from the water-gas shift reaction. Catalytic dehydrogenation was investigated by feeding only C_3H_8 to the catalyst bed containing the five-cycle H_2 catalyst. During this test, H_2 and C_3H_6 both formed at

DOI: 10.1021/cs501265b
ACS Catal. 2015, 5, 1344−1352

approximately one-third of their rate during ODHP, and their rates steadily decreased with time on stream, likely due to coking. The high selectivity observed under the O_2-lean reaction conditions likely was a combined effect of ODHP (until the O_2 was depleted) and catalytic dehydrogenation.

Turnover frequencies, given in Table 3, were measured after achieving steady state at 673 K at less than full O_2 conversion at 673 K and were the highest for the smallest particles and decreased with particle size. In a study on clusters of 8−-10 Pt atoms by Vajda et al., the Pt catalysts achieved TOFs of ∼0.8 s^{-1} at 673 K, where the TOF was reported per *total* Pt atom.[9] The ALD catalysts reported here had TOFs intermediate between those of Vajda's catalysts and Pt monoliths tested with extremely short contact times (with a TOF of 0.01 s^{-1}); because the TOFs in Table 3 are based on catalysts having computed dispersions at or near 100% (Table 2), these TOFs are directly comparable to those of Vajda.[10] The selectivities for all catalysts (when run at less than 100% O_2 conversion) were lower than those for runs under the O_2-lean conditions, likely because more O_2 was available for C_3H_6 and C_3H_8 combustion.

Table 3. Catalytic ODHP Performance at 673 K

catalyst	C_3H_6 TOF[a] (mol of C_3H_6 (mol of $Pt_{surface}$)$^{-1}$ s^{-1})	C_3H_6 selectivity (%)	C_3H_8 conversion (%)
1-cycle Pt ALD with H_2	0.42 ± 0.03	18	6.4
1-cycle Pt ALD with O_2	0.43 ± 0.04	13	6.3
5-cycle Pt ALD with H_2	0.26 ± 0.04	7.4	7.7
5-cycle Pt ALD with O_2	0.11 ± 0.02	7.0	6.9

[a]Errors of the TOFs reported above are representative of error in measuring the catalyst weight.

CONCLUSIONS

Supported Pt nanoparticles between ∼1 and 2.5 nm were synthesized by varying the ALD chemistry (O_2 or H_2 as the second precursor) and the number of cycles used. These catalysts were selective for oxidative dehydrogenation of propane, with the smallest particles having the highest C_3H_6 formation TOFs. The differences between the second half-reaction chemistries used to produce these catalysts were probed via in situ IR, which showed gradual depletion of OH groups when H_2 was used but relatively little change when the ALD was done with O_2. The concentration of low-coordination Pt atoms was also found to vary with particle size using CO DRIFTS and CO TPD. The catalysts with more low-coordination Pt atoms (identified by CO DRIFTS) had higher ODHP selectivity and TOF at 673 K, but at lower temperatures trends with coordination number were less apparent. The smallest catalyst particles had a maximum selectivity of 37% and a maximum TOF to C_3H_6 of ∼0.42 s^{-1}. These small particle sizes are achievable through the facile ALD synthesis, and these ALD catalysts had much higher TOFs than mostly Pt(111)-terminated surfaces.

ASSOCIATED CONTENT

Supporting Information

The following file is available free of charge on the ACS Publications website at DOI: 10.1021/cs501265b.

Additional CO DRIFTS spectra, CO TPD, and reaction data (PDF)

AUTHOR INFORMATION

Corresponding Author

*E-mail for J.W.M.: Will.Medlin@Colorado.edu.

Notes

The authors declare no competing financial interest.

ACKNOWLEDGMENTS

The authors acknowledge support from the National Science Foundation award CBET 0854251. The authors acknowledge the support for imaging particles from both Tom Giddings at the MCDB Bio3d Electron microscopy center and Aric Sanders at the National Institute of Standard's PIF facility in Boulder. We also thank Dr. Simon Pang for assistance with CO DRIFTS experiments.

REFERENCES

(1) Somorjai, G. A.; Frei, H.; Park, J. Y. . *J. Am. Chem. Soc.* **2009**, *131*, 16589−16605.
(2) Somorjai, G. A.; York, R. L.; Butcher, D.; Park, J. Y. *Phys. Chem. Chem. Phys.* **2007**, *9*, 3500−3513.
(3) Li, Y.; Somorjai, G. A. *Nano Lett.* **2010**, *10*, 2289−2295.
(4) Hu, E. L.; Davis, S. M.; Davis, R.; Scher, E. *Applications: Catalysis by Nanostructured Materials: Nanotechnology Research Directions for Societal Needs in 2020*. Springer: Dordrecht, The Netherlands, 2011; Vol. *1*, pp 445−466.
(5) Ceresana Market Study: Propylene (UC-1705). http://www.ceresana.com/en/market-studies/chemicals/propylene/propylene-market-share-capacity-demand-supply-forecast-innovation-application-growth-production-size-industry.html (accessed 12−13−13).
(6) Corma, A.; Melo, F.; Sauvanaud, L.; Ortega, F. *Catal. Today* **2005**, *107*, 699−706.
(7) Cavani, F.; Ballarini, N.; Cericola, A. *Catal. Today* **2007**, *127*, 113−131.
(8) Van Santen, R. A. *Acc. Chem. Res.* **2008**, *42*, 57−66.
(9) Vajda, S.; Pellin, M. J.; Greeley, J. P.; Marshall, C. L.; Curtiss, L. A.; Ballentine, G. A.; Elam, J. W.; Catillon-Mucherie, S.; Redfern, P. C.; Mehmood, F.; Zapol, P. *Nat. Mater.* **2009**, *8*, 213−216.
(10) Silberova, B.; Fathi, M.; Holmen, A. *Appl. Catal., A* **2004**, *276*, 17−28.
(11) Gharibi, M.; Zangeneh, F. T.; Yaripour, F.; Sahebdelfar, S. *Appl. Catal., A* **2012**, *443−444*, 8−26.
(12) Somorjai, G. A.; Borodko, Y. G. *Catal. Lett.* **2001**, *76*, 1−5.
(13) Aiken Iii, J. D.; Finke, R. G. *J. Mol. Catal. A: Chem.* **1999**, *145*, 1−44.
(14) Bozon-Verduraz, F.; Fiévet, F.; Piquemal, J.-Y.; Brayner, R.; El Kabouss, K.; Soumare, Y.; Viau, G.; Shafeev, G. *Braz. J. Phys.* **2009**, *39*, 134−140.
(15) Aaltonen, T.; Ritala, M.; Sajavaara, T.; Keinonen, J.; Leskela, M. *Chem. Mater.* **2003**, *15*, 1924−1928.
(16) Christensen, S. T.; Elam, J. W.; Rabuffetti, F. A.; Ma, Q.; Weigand, S. J.; Lee, B.; Seifert, S.; Stair, P. C.; Poeppelmeier, K. R.; Hersam, M. C.; Bedzyk, M. J. *Small* **2009**, *5*, 750−757.
(17) Li, J.; Liang, X.; King, D. M.; Jiang, Y.-B.; Weimer, A. W. *Appl. Catal., B* **2010**, *97*, 220−226.
(18) Zhou, Y.; King, D. M.; Liang, X.; Li, J.; Weimer, A. W. *Appl. Catal., B* **2010**, *101*, 54−60.
(19) Setthapun, W.; Williams, W. D.; Kim, S. M.; Feng, H.; Elam, J. W.; Rabuffetti, F. A.; Poeppelmeier, K. R.; Stair, P. C.; Stach, E. A.; Ribeiro, F. H.; Miller, J. T.; Marshall, C. L. *J. Phys. Chem. C* **2010**, *114*, 9758−9771.
(20) Kessels, W.; Knoops, H.; Dielissen, S.; Mackus, A.; van de Sanden, M. *Appl. Phys. Lett.* **2009**, *95*, 013114.

DOI: 10.1021/cs501265b
ACS Catal. 2015, 5, 1344−1352

(21) Aaron Deskins, N.; Mei, D.; Dupuis, M. *Surf. Sci.* **2009**, *603*, 2793−2807.
(22) Corral Valero, M.; Raybaud, P.; Sautet, P. *J. Phys. Chem. B* **2006**, *110*, 1759−1767.
(23) King, D. M.; Spencer Ii, J. A.; Liang, X.; Hakim, L. F.; Weimer, A. W. *Surf. Coat. Technol.* **2007**, *201*, 9163−9171.
(24) Gould, T. D.; Lubers, A. M.; Neltner, B. T.; Carrier, J. V.; Weimer, A. W.; Falconer, J. L.; Will Medlin, J. W. *J. Catal.* **2013**, *303*, 9−15.
(25) Mackus, A. J. M.; Leick, N.; Baker, L.; Kessels, W. M. M. *Chem. Mater.* **2012**, *24*, 1752−1761.
(26) Miller, K. L.; Lee, C. W.; Falconer, J. L.; Medlin, J. W. *J. Catal.* **2010**, *275*, 294−299.
(27) Kip, B. J.; Duivenvoorden, F. B. M.; Koningsberger, D. C.; Prins, R. *J. Catal.* **1987**, *105*, 26−38.
(28) Parsons, G. N.; George, S. M.; Knez, M. *MRS Bulletin* **2011**, *36*, 865−871.
(29) Kappers, M. J.; Maas, J. H. *Catal. Lett.* **1991**, *10*, 365−373.
(30) Lebedeva, N.; Rodes, A.; Feliu, J.; Koper, M.; Van Santen, R. *J. Phys. Chem. B* **2002**, *106*, 9863−9872.
(31) De Graaf, J.; Van Dillen, A.; De Jong, K.; Koningsberger, D. . *Catal.* **2001**, *203*, 307−321.
(32) Lundwall, M. J.; McClure, S. M.; Goodman, D. W. *J. Phys. Chem. C* **2010**, *114*, 7904−7912.
(33) Tanksale, A.; Beltramini, J. N.; Dumesic, J. A.; Lu, G. Q. *J. Catal.* **2008**, *258*, 366−377.
(34) Zafiris, G. S.; Gorte, R. J. *J. Catal.* **1993**, *140*, 418−423.
(35) Xu, J.; Yates, J. T., Jr. *Surf. Sci.* **1995**, *327*, 193−201.
(36) Foger, K.; Anderson, J. R. *Appl. Surf. Sci.* **1979**, *2*, 335−351.
(37) Qiao, B.; Wang, A.; Yang, X.; Allard, L. F.; Jiang, Z.; Cui, Y.; Liu, J.; Li, J.; Zhang, T. *Nat. Chem.* **2011**, *3*, 634−641.
(38) Kwak, J. H.; Hu, J.; Mei, D.; Yi, C.-W.; Kim, D. H.; Peden, C. H. F.; Allard, L. F.; Szanyi, J. *Science* **2009**, *325*, 1670−1673.
(39) McCabe, R. W.; Schmidt, L. D. *Surf. Sci.* **1977**, *66*, 101−124.
(40) Jackson, S. D.; Glanville, B. M.; Willis, J.; McLellan, G. D.; Webb, G.; Moyes, R. B.; Simpson, S.; Wells, P. B.; Whyman, R. . *Catalysis* **1993**, *139*, 207−220.
(41) Lei, Y.; Liu, B.; Lu, J.; Lobo-Lapidus, R. J.; Wu, T.; Feng, H.; Xia, X.; Mane, A. U.; Libera, J. A.; Greeley, J. P.; Miller, J. T.; Elam, J. W. *Chem. Mater.* **2012**, *24*, 3525−3533.

DOI: 10.1021/cs501265b
ACS Catal. 2015, 5, 1344−1352